Available online at www.sciencedirect.com
SCIENCE DIRECT®
International Journal of Heat and Mass Transfer 48 (2005) 1858–1867
International Journal of HEAT and MASS TRANSFER
www.elsevier.com/locate/ijhmt

Three-dimensional numerical computation for magnetic convection of air inside a cylinder heated and cooled isothermally from a side wall

P. Filar [a], E. Fornalik [b,c], M. Kaneda [a,b], T. Tagawa [a,b], H. Ozoe [a,b,*], J.S. Szmyd [c]

[a] *Interdisciplinary Graduate School of Engineering Sciences, Kyushu University, Kasuga 816-8580, Japan*
[b] *Institute for Materials Chemistry and Engineering, Kyushu University, 6-1 Kasuga Koen, Kasuga 816-8580, Japan*
[c] *AGH University of Science and Technology, 30-059 Krakow, Poland*

Received 18 February 2004

Abstract

Three-dimensional convection of air in a vertical cylinder isothermally heated and cooled from a side wall was numerically computed both in magnetic and gravity fields. A single electric coil was placed around a cylinder to generate a magnetic field. Convection was calculated for various coil levels and magnetic strengths. The gravity field, magnetic strength and Rayleigh number are shown to have substantial effect. Convection modes and heat transfer rates are also presented.

Keywords: Natural convection; Magnetizing force; Numerical analysis; Cylindrical enclosure; Air

1. Introduction

Recently, various new phenomena due to magnetizing force have been reported under a strong magnetic field of a super-conducting magnet. Magnetic field as large as 10–20 T can be steadily produced around the 10 cm diameter bore space kept in a room temperature. The phenomena due to the magnetizing force had been known for many years [1,2] but almost totally neglected until the super-conducting magnet became available.

In such strong magnetic fields, the convection of paramagnetic gases like oxygen or diamagnetic fluids like water, have been reported to be affected. For example, Braithwaite et al. [3] investigated convection of gadolinium nitrate water solution (paramagnetic) in the configuration of Rayleigh–Bénard system under a magnetic field. They described the suppression or enhancement of the natural convection heat transfer rate due to the magnetic field. Oxygen gas has relatively high magnetic susceptibility among gases and is typically used for those experiments due to its paramagnetic behavior in accordance with Curie's law. Wakayama and coworkers [4–8] have been very active in finding

* Corresponding author. Address: Institute for Materials Chemistry and Engineering, Kyushu University, 6-1 Kasuga Koen, Kasuga 816-8580, Japan. Tel.: +81 92 583 7834; fax: +81 92 583 7838.
E-mail address: ozoe@cm.kyushu-u.ac.jp (H. Ozoe).

0017-9310/$ - see front matter © 2005 Elsevier Ltd. All rights reserved.
doi:10.1016/j.ijheatmasstransfer.2004.10.034

Nomenclature

$\mathbf{b} = (b_r, 0, b_z)$ magnetic induction (T = Wb/m^2 = V s/m^2)
b_0 reference magnetic induction, $\mu_m i/r_0$ (T)
$\mathbf{B} = (B_r, 0, B_z)$ dimensionless magnetic induction, $\mathbf{b}/b_0$ (–)
c_p specific heat (J/(kg K))
d_c electric coil diameter (m)
$\mathbf{f}_{buoy} = g\rho_0\beta(\theta - \theta_0)$ $[(0,0,1)^T]$ gravitational buoyancy force (N/m^3)
$\mathbf{f}_{mag} = \chi_{m0}\beta(\theta - \theta_0)\nabla\mathbf{b}^2/\mu_m$ magnetizing buoyancy force (N/m^3)
$\mathbf{F}_{buoy} = RaPrT$ $[(0,0,1)^T]$ dimensionless buoyancy force (–)
$\mathbf{F}_{mag} = -RaPrT\gamma\nabla\mathbf{B}^2$ dimensionless magnetizing buoyancy force (–)
g gravitational acceleration (m/s^2)
h cylinder height (m)
H dimensionless height, (aspect ratio) h/r_0 (–)
i electric current (A)
l vertical length (m)
L dimensionless vertical length, l/r_0 (–)
$Nu = Q_{convection}/Q_{conduction}$ average Nusselt number (–)
p pressure (Pa)
p_0 reference pressure, $\rho_0 u_0^2$ (Pa)
P dimensionless pressure, p/p_0 (–)
$Pr = \nu/\alpha$ Prandtl number (–)
Q heat flux (W/m^2)
r_0 reference length, (cylinder radius) (m)
r, z radial and axial coordinates (m)
R, Z dimensionless radial and axial coordinates, $(r,z)/r_0$ (–)
$\mathbf{r}$ position vector (m)
r_c electric coil radius (m)
R_c dimensionless electric coil radius, r_c/r_0 (–)
$Ra = g\beta(\theta_{hot} - \theta_{cold})r_0^3/(\alpha\nu)$ Rayleigh number (–)
$\mathbf{s}$ a periphery line of a coil (m)
$\mathrm{d}\mathbf{s}$ tangential vector of an infinitesimal coil element (m)
t time (s)
t_0 reference time, r_0/u_0 (s)
$T = (\theta - \theta_0)/(\theta_{hot} - \theta_{cold})$ dimensionless temperature (–)
u_0 reference velocity, α/r_0 (m/s)
$\boldsymbol{v} = (u, v, w)$ velocity vector components (m/s)
$\boldsymbol{V} = (U, V, W)$ dimensionless velocity, $(u,v,w)/u_0$, (–)
Z_c coil elevation (–)

Subscripts
buoy buoyancy
mag magnetizing
0 reference value
hot heating zone temperature
cold cooling zone temperature
init initial condition
r, z r, z components of vector

Greek symbols
α thermal diffusivity of air (m^2/s)
β thermal expansion coefficient (K^{-1})
$\gamma = (\chi_{m0} b_0^2)/(\rho_0\mu_m g r_0)$ magnetic field strength parameter (–)
μ viscosity (Pa s)
λ thermal conductivity (W/(m K))
μ_m magnetic permeability (H/m) = (Wb/(A m))
ν kinematic viscosity, μ/ρ_0 (m^2/s)
θ temperature (K)
$\theta_0 = (\theta_{hot} + \theta_{cold})/2$ reference temperature (K)
$\Delta\theta = \theta_{hot} - \theta_{cold}$ temperature difference (K)
ρ density (kg/m^3)
ρ_0 reference density at θ_0 (kg/m^3)
τ dimensionless time, t/t_0 (–)
χ_m magnetic susceptibility of air (–)
χ_{m0} reference magnetic susceptibility of air at θ_0 (–)
ψ angular coordinate (rad)

various interesting phenomena, such as jet stream of nitrogen gas into air (Wakayama jet) in a steeply decreasing magnetic field, enhancement of combustion flames and sustaining flame under microgravity. Kitazawa and coworkers [9,10] have presented many interesting phenomena occurred in the magnetic field i.e. the levitation of a water droplet by strong magnetic field, driving of air flow due to magnetic field etc. Ozoe and coworkers [11–14] reported a number of numerical calculations for natural ventilation and natural convection in a magnetically cancelled field against gravity acceleration. However, the three-dimensional analysis of air convection in a vertical cylinder being cooled and heated from a side wall has not been yet fully presented under a strong magnetic field. The present paper describes numerical analysis of the air convection inside a cylinder where the upper and lower part of the cylinder side walls are isothermally cooling and heating zones, while the intermediate section and top and bottom plates are thermally adiabatic. This configuration is similar to a thermosyphon system. The level of magnetic coil around the cylinder was studied in order to investigate the convection phenomena in detail.

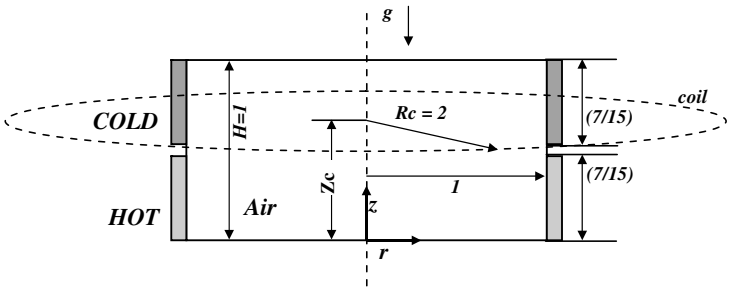

Fig. 1. The system geometry. A vertical cross-section of a cylinder.

2. Modeled system and equations

Modeled system is shown in Fig. 1. It is a vertical cylinder heated from a lower side wall and cooled from an upper side wall. The vertical length of heating and cooling zones is $L = (7/15)$, respectively. The area in-between ($L = (1/15)$) and top and bottom plates of the cylinder are thermally insulated. The aspect ratio of cylinder ($H = h/r_0$) was set to be equal to 1 as drawn schematically in Fig. 1. The coil radius R_c was arbitrarily set to be double of the cylinder radius.

The fluid was assumed to be paramagnetic, incompressible and Newtonian. Boussinesq approximation was employed for both gravity and magnetizing force terms. Magnetic field distribution was obtained from integration of Biot–Savart's law for the whole computational domain.

The governing equations for the considered system can be written as follows in nondimensional variables, according to Tagawa et al. [14] and Bai et al. [15]:

$$\mathbf{V}\cdot\mathbf{V} = 0 \tag{1}$$

$$\frac{\mathrm{D}T}{\mathrm{D}\tau} = \nabla^2 T \tag{2}$$

$$\frac{\mathrm{D}\mathbf{V}}{\mathrm{D}\tau} = -\nabla P + Pr\nabla^2\mathbf{V} + RaPrT\left[-\gamma\nabla\mathbf{B}^2 + \begin{pmatrix}0\\0\\1\end{pmatrix}\right] \tag{3}$$

$$\mathbf{B} = \frac{1}{4\pi}\oint_{\text{coil}}\frac{\mathrm{d}\mathbf{S}\times\mathbf{R}}{\mathbf{R}^3} \tag{4}$$

The initial and boundary conditions are:

At $\tau = 0$, $\mathbf{V} = \mathbf{0}$, $T = 0$ for $0 \leqslant R \leqslant 1.0$, $Z = 0$, $Z = 1.0$ (adiabatic bottom and top cylinder plates)

$$\mathbf{V} = \mathbf{0}, \quad \partial T/\partial Z = 0$$

for $R = 1$, $0 \leqslant Z \leqslant 7/15$ (cylinder wall–heating zone)

$$\mathbf{V} = \mathbf{0}, \quad T = +0.5$$

for $R = 1$, $7/15 < Z < 8/15$ (cylinder wall–adiabatic zone)

$$\mathbf{V} = \mathbf{0}, \quad \partial T/\partial R = 0$$

for $R = 1$, $8/15 \leqslant Z \leqslant 1$ (cylinder wall–cooling zone)

$$\mathbf{V} = \mathbf{0}, \quad T = -0.5$$

These equations were approximated with finite difference equations and numerically solved with using the three-dimensional HSMAC algorithm. Continuity equation, coupled momentum equations and energy equation were solved in iterative process. A third order upwind scheme was applied to the inertial terms. Computations were carried out for staggered grid systems to satisfy the equation of continuity in each grid cell. The grid numbers applied to the system were 16, 36 and 32 along the R, ψ and Z directions, respectively. These grid numbers were selected from the previous accuracy tests for various grids based on two- dimensional calculations [16]. Grid was taken finer near the system boundaries and coarser in the center. The mathematical problem of computational singularity at the radial center was circumvented by the technique of Ozoe and Toh [17].

3. Numerical results and discussion

The contour lines of a square magnetic induction $\mathbf{B}^2$ and its gradient $\nabla\mathbf{B}^2$ vector are shown in Fig. 2 for a coil location, $Z_c = 1$. Computations were carried out for the air convection in a cylinder with an electric coil located at various levels $0 \leqslant Z_c \leqslant 1$. The physical properties of air and reference dimensional values are listed in Table 1.

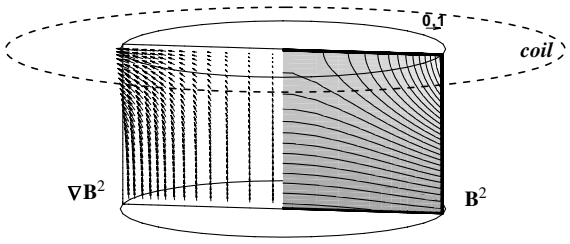

Fig. 2. The contour lines of $\mathbf{B}^2$ on the right-hand side and its gradient vectors $\nabla\mathbf{B}^2$ on the left-hand side in a vertical cross-section of a cylinder for a coil located at $Z_c = 1$.

Table 1
Thermophysical data applied in the calculations and physical properties of air at $\theta = 300$ K and $p = 0.1013$ MPa—[18]

$b_0 = 3.1$ T
$r_c = 0.05$ m
$\chi_{m0} = 3.77 \times 10^{-7}$
$\mu_m = 4\pi \times 10^{-7}$ H/m
$\rho_0 = 1.176$ kg/m^3
$c_p = 1.007 \times 10^3$ J/(kg K)
$\alpha = 22.15 \times 10^{-6}$ m^2/s
$\lambda = 26.23 \times 10^{-3}$ W/(m K)
$\nu = 1.578 \times 10^{-5}$ m^2/s
$r_0 = 0.025$ m
$\beta = 3.462 \times 10^{-3}$ K^{-1}
$\mu = 1.856 \times 10^{-5}$ Pa s
$\Delta\theta = 10$ K

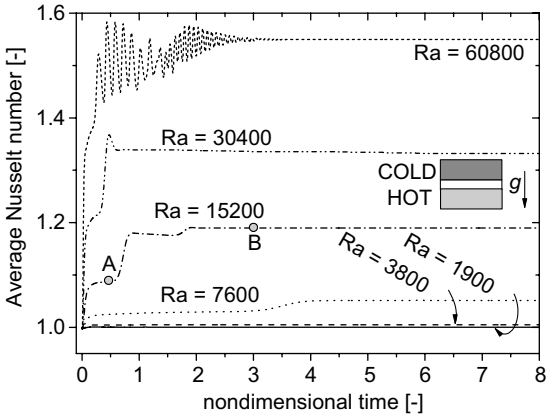

Fig. 3. Transient responses of Nusselt number in a gravity field at $Pr = 0.71$, $\gamma = 0$ and $Ra = 1.9 \times 10^3$, 3.8×10^3, 7.6×10^3, 1.52×10^4, 3.04×10^4, 6.08×10^4, respectively.

3.1. Without magnetic field

At first the Rayleigh number was varied while magnetic field was not applied. Fig. 3 shows the transient responses of the average Nusselt number for the various Rayleigh numbers 1.9×10^3–6.08×10^4 at $\gamma = 0$ (no magnetic field). The converged average Nusselt numbers are listed in Table 2. At $Ra = 1.52 \times 10^4$ flow mode becomes axisymmetric at $\tau = 0.5$ (point A) and full 3D flow after $\tau = 3.0$ (point B).

Table 2
Computed average Nusselt number at $\gamma = 0$ and $Pr = 0.71$

Ra	1900	3800	5000	6000	7600	15200	30400	60800
Nu	≈1.0	1.005	1.015	1.023	1.051	1.190	1.332	1.550

Fig. 4 presents isothermal contours and velocity profiles at $\gamma = 0$, $Pr = 0.71$ and $Ra = 1.52 \times 10^4$. Fig. 4(a) shows two-dimensional, axi-symmetric mode at $\tau = 0.5$. Fig. 4(b) and (c) show 3D flow at $\tau = 3$. They are in two perpendicular, vertical planes either along the X or Y axis, respectively. These figures show that flow mode is no more axi-symmetric. This system is unstable in a gravity field and convection should start immediately when Rayleigh number differs from zero. However, when we plot, Nu vs. Ra, as shown in Fig. 5, abrupt increase occurs in the Nusselt number at $Ra \approx 6000$. This is similar to the classical Rayleigh instability at the critical Rayleigh number. We tentatively called this as a quasi-critical Rayleigh number Ra_c. Similar characteristics may be expected for other geometries of the enclosure and aspect ratios, etc.

In Fig. 6 four streaklines with two horizontal isothermal contours at (a) $Z = 0.45$ and (b) $Z = 0.55$ at a non-magnetic case can be seen. In (c) the isothermal contours are shown along the cylinder wall at radius $R = 0.9$ at $Pr = 0.71$, $Ra = 1.52 \times 10^4$ and $\tau = 3.0$ which corresponds to $t = 85$ [s] for the dimensional system of Table 1. The isothermal contours represent the asymmetric flow mode with two upflow columns of fluid and two downflow. The isothermal contours at the heights $Z = 0.45$ and 0.55 appear to be shifted in the circumferential direction at about $\pi/2$ radians, although the streaklines are in the same direction which suggests the same flow mode.

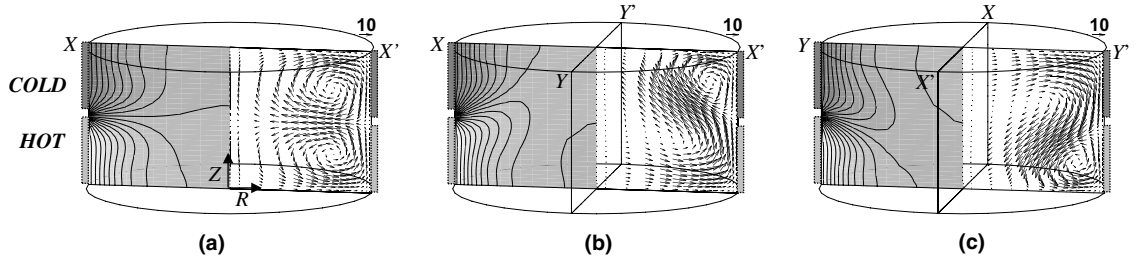

Fig. 4. Isothermal contours and velocity profiles in gravity field at $\gamma = 0$, $Pr = 0.71$ and $Ra = 1.52 \times 10^4$: (a) mode A at $\tau = 0.5$ and in a X–X' plane, (b) mode B at $\tau = 3.0$ and in a X–X' plane, (c) mode B at $\tau = 3.0$ and in a Y–Y' plan.

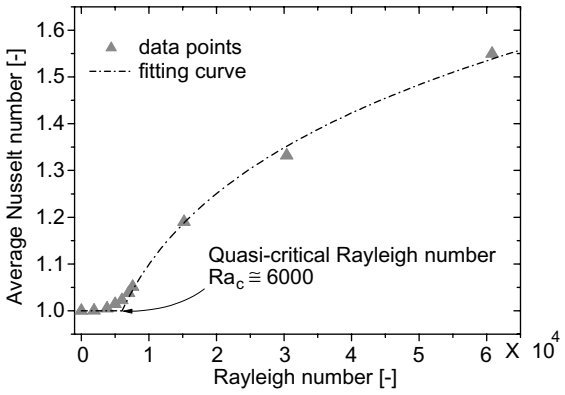

Fig. 5. Computed average Nusselt number vs. Rayleigh number in gravity field at $\gamma = 0$ and $Pr = 0.71$.

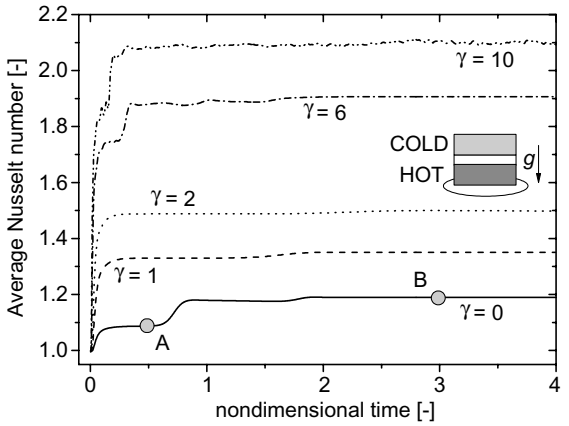

Fig. 7. Transient responses of the average Nusselt number in gravity field at $Z_c = 0$, $Pr = 0.71$, $Ra = 1.52 \times 10^4$ and $\gamma = 0$, 1, 2, 6, 10, respectively.

3.2. In the magnetic field

Fig. 7 shows the transient responses of the average Nusselt number with the coil located at $Z_c = 0$ and at $Pr = 0.71$, $Ra = 1.52 \times 10^4$ for $\gamma = 0$, 1, 2, 6 and 10. The average Nusselt number becomes about twice at $\gamma = 10$ than that at $\gamma = 0$. At $\gamma = 10$ and higher, convection became oscillatory. Then, similar computations were carried out for various heights of a coil location Z_c. Table 3 lists the average Nusselt number for the combination of the Rayleigh numbers and the height of a coil location Z_c, at $\gamma = 10$ and $Pr = 0.71$. They are shown in Fig. 8. Both coil elevation and Rayleigh number affect the heat transfer rate extensively. The maximum Nusselt number could be obtained for the coil located at about $Z_c = 0.4$. For top location of coil $Z_c = 1.0$ the effect of Rayleigh number becomes negligible.

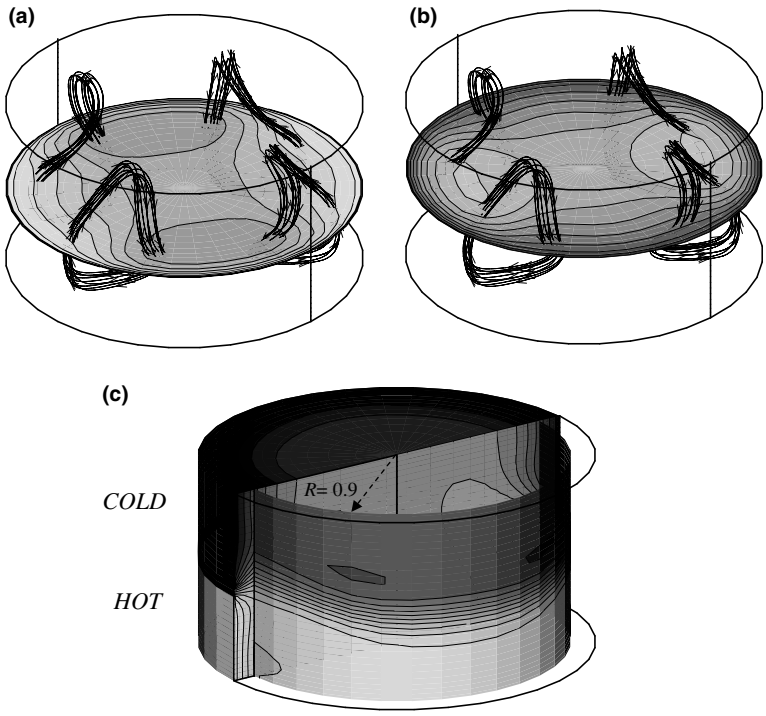

Fig. 6. Temperature contours and streaklines in a non-magnetic field $\gamma = 0$. Isotherms in two horizontal sections (a) $Z = 0.45$, (b) $Z = 0.55$ and (c) isothermal contours at ($R = 0.9$). $Pr = 0.71$ and $Ra = 1.52 \times 10^4$.

Table 3
The effect of the Rayleigh number and coil location Z_c on the average Nusselt numbers at $\gamma = 10$ and $Pr = 0.71$

Z_c	Ra		
	3800	15,200	60,800
0	1.675	2.121 ± 0.020	3.004 ± 0.091
0.25	1.961	2.651	3.655
0.5	1.872	2.624	3.699
0.75	1.352	1.604	1.915
1	1.098	1.178	1.291

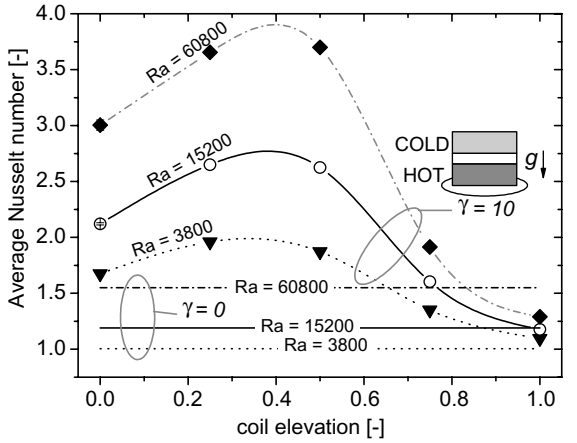

Fig. 8. The average Nusselt number in gravity field vs. coil location Z_c, at $Pr = 0.71$, $\gamma = 10$ and $Ra = 0.38 \times 10^4$, 1.52×10^4 and 6.08×10^4, respectively.

Fig. 9 shows the isothermal contours and velocity vectors at $Ra = 0.38 \times 10^4$, 1.52×10^4 and 6.08×10^4 and at two levels of coil $Z_c = 0.25$ and $Z_c = 0.75$. The reference magnitude for the velocity vectors are changed due to large difference between them. Although axisymmetric flow was resulted in all cases, the effect of coil location and Rayleigh number is extensive.

3.3. Effect of coil location and γ parameter

Fig. 10 shows the average Nusselt numbers vs. coil location Z_c at $Pr = 0.71$ and $Ra = 1.52 \times 10^4$ with a parameter $\gamma = 0$, 1, 10, and 100. For $Z_c = 0$ additional results are plotted for $\gamma = 2$ and 6. The heat transfer rate increases with the strength of the magnetic field γ and attains local maximum near $Z_c = 0.4$. At $\gamma = 1$ the Nusselt number depends on Z_c almost symmetrically about the middle height $Z_c = 0.5$. At $\gamma = 10$ and 100 oscillations were resulted at $Z_c = 0$. The Nusselt number takes large values at $Z_c = 0$ but almost conduction state is resulted

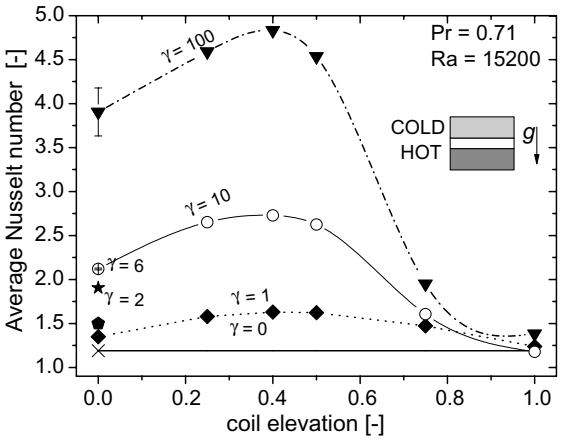

Fig. 10. The average Nusselt number value in a gravity field ($g = 9.81$ m/s^2) vs. coil location Z_c, at $Pr = 0.71$, $Ra = 1.52 \times 10^4$ and at $\gamma = 0$, 1, 10, and 100, respectively.

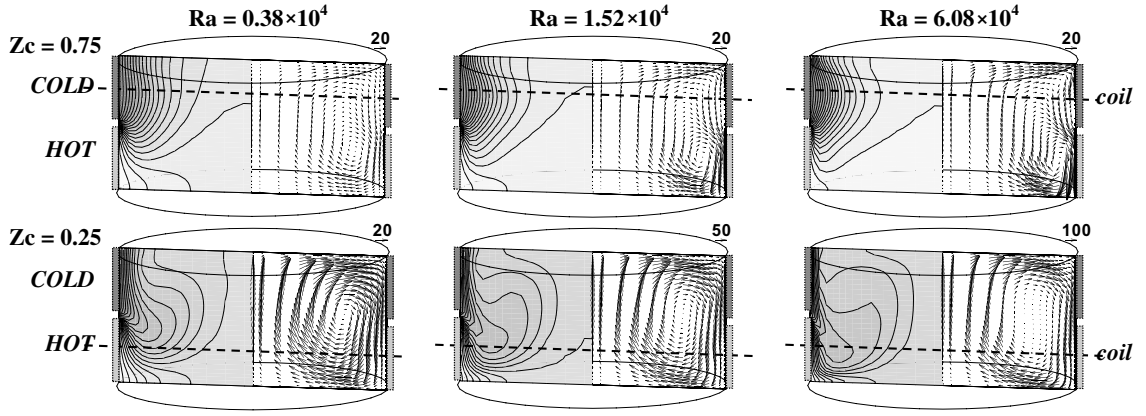

Fig. 9. Isothermal contours and velocity profiles in gravity field at $\gamma = 10$, $Pr = 0.71$ and $Ra = 0.38 \times 10^4$, 1.52×10^4 and 6.08×10^4 respectively. Upper rows are at $Z_c = 0.75$ and lower at $Z_c = 0.25$.

Table 4
The effect of coil location Z_c and magnetic strength γ on the average Nusselt number at $Pr = 0.71$ and $Ra = 1.52 \times 10^4$

Z_c	γ			
	0	1	10	100
0	1.190	1.350	2.121 ± 0.020	3.905 ± 0.27
0.25	1.190	1.579	2.651	4.591
0.4	1.190	1.630	2.728	4.834
0.5	1.190	1.622	2.624	4.537
0.75	1.190	1.472	1.604	1.951
1	1.190	1.239	1.178	1.384

at $Z_c = 1$ where the cold air is trapped by magnetic field near the top cooling plate. These Nusselt numbers are listed in Table 4.

Fig. 11 shows force vectors $-T\,[\gamma\nabla\mathbf{B}^2 - (0,0,1)^{\mathrm{T}}]$ on the right hand side of each diagram and isothermal contours on the left hand side at $Pr = 0.71$ and $Ra = 1.52 \times 10^4$. Graphs are for combinations of $\gamma = 0$, 1, 10 and 100 and $Z_c = 0$, 0.5 and 1, respectively. Corresponding velocity vectors and temperature distributions are also presented in Fig. 12. Magnitudes of reference vectors are listed at the top right corner of each graph and changed depending on the location of the coil.

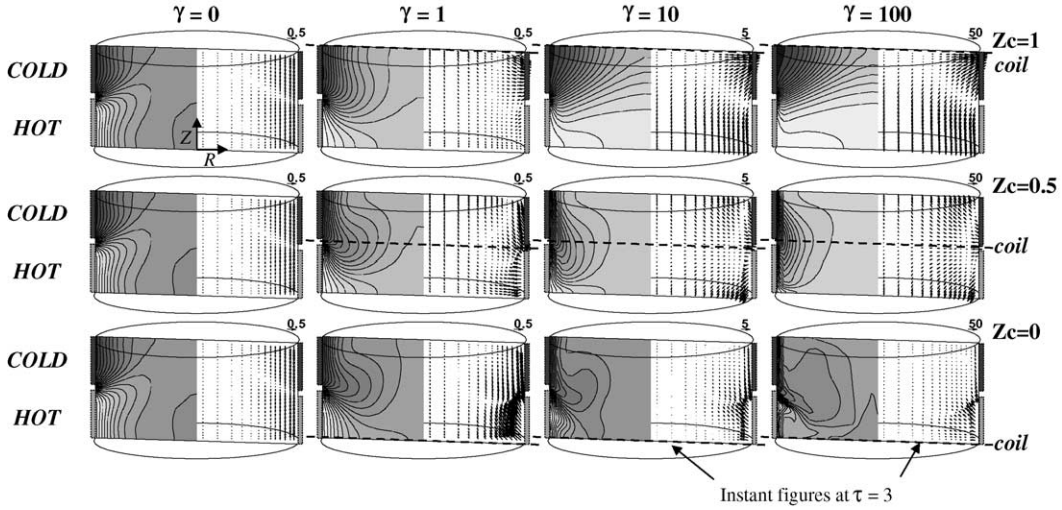

Fig. 11. Isothermal contours and force vectors $-T[\gamma\nabla\mathbf{B}^2 - (0,0,1)^{\mathrm{T}}]$ at $\gamma = 0$, 1, 10, 100 and for $Z_c = 0$, 0.5 and 1, at $Pr = 0.71$ and $Ra = 1.52 \times 10^4$.

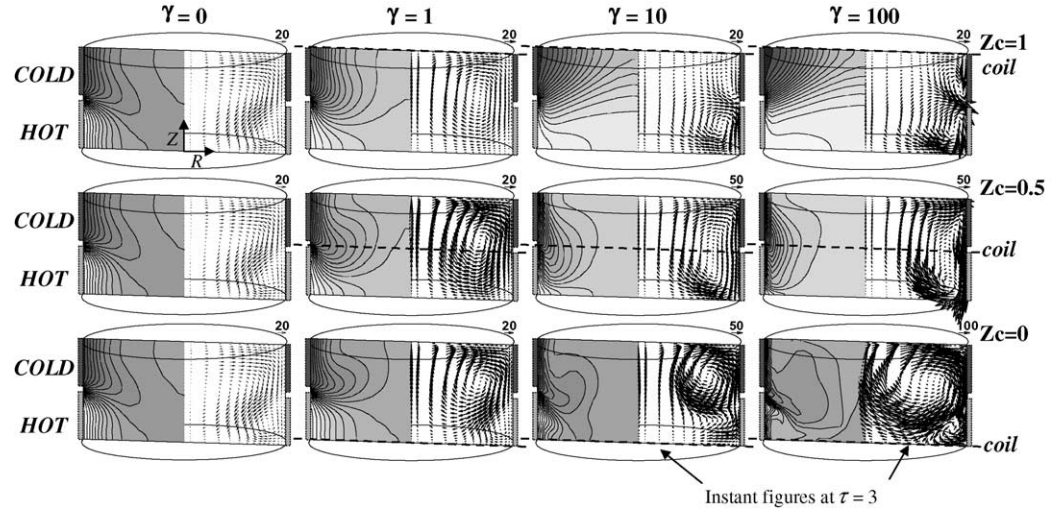

Fig. 12. Isothermal contours and velocity profiles at $\gamma = 0$, 1, 10, 100 and for $Z_c = 0$, 0.5 and 1, at $Pr = 0.71$ and $Ra = 1.52 \times 10^4$.

For weak magnetic field $\gamma = 1$, the flow mode is almost unaffected by the coil location although they are different from those at $\gamma = 0$. At $\gamma = 1$, magnetizing force is not strong enough to suppress natural convection in the top part of cylinder which results in one global vortex through all the cylinder as seen in Fig. 12. For the top location of coil $Z_c = 1$, a reverse flow in comparison to natural convection can be observed. It appears due to strong effect of magnetizing force which tends to attract the cold air from the upper cooling zone towards the top corner, where the gradient of square magnetic induction is large as shown in Fig. 11. As γ becomes large, the temperature stratification is resulted for the present system cooled from upper side wall at $\gamma = 10$ and 100. Simultaneously hot fluid near the lower heating zone is repelled downwards due to its low magnetic susceptibility. For a coil located in the middle height of cylinder ($Z_c = 0.5$) a single vortex was calculated with strong convection near side wall as seen in Fig. 12. For the bottom location of coil ($Z_c = 0$), cold air from the top part of enclosure is driven downwards both by buoyancy and magnetizing forces. In the consequence, very intensive circulation is resulted. Such configuration seems to be very effective for the fluid mixing. At $\gamma = 10$ and 100 non-periodic oscillations were resulted which is also indicated by the error bars in the Nusselt number graph in Fig. 10. Because of this oscillation only instant profiles at $\tau = 3$ are drawn for those cases. At these conditions ($\gamma \geqslant 10$, $Z_c = 0$, $Ra = 1.52 \times 10^4$, $Pr = 0.71$) cold air from the top is attracted downwards but simultaneously hot fluid from the bottom is pushed upwards. These counter effects seem to cause the flow instability.

Fig. 13(a)–(d) are horizontal cross sections of isotherms at $\gamma = 0$, 1, 2 and 6 taken at level $Z = 0.18$ and corresponding vertical cross section along A–B line in the right hand side. Flow symmetry was broken at $Z_c = 0$ and three-dimensional results were obtained. These structures occurred for $10 \geqslant \gamma \geqslant 1$ with coil at $Z_c = 0$ and are localized in the bottom part of cylinder where upward flow collides with downward flow. Depending on the strength of magnetic field, several spoke numbers were obtained. Primarily, the number of spokes obtained at $\gamma = 0$ increases with γ. Namely,

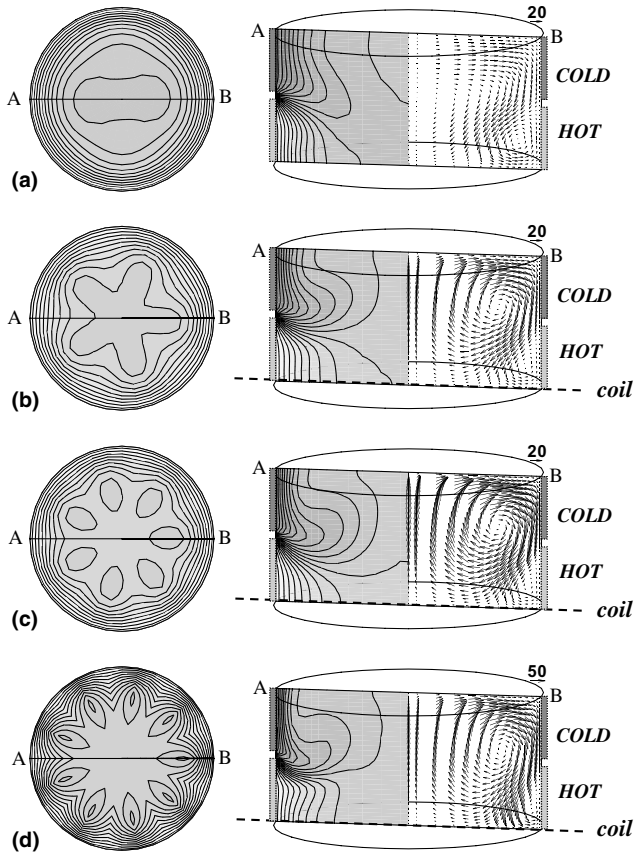

Fig. 13. Isothermal contours in a plane $Z = 0.18$ (left-hand side) and at $Z_c = 0$, $Pr = 0.71$ and $Ra = 1.52 \times 10^4$. (a) $\gamma = 0$, (b) $\gamma = 1$, (c) $\gamma = 2$ and (d) $\gamma = 6$. The right hand diagrams are corresponding isotherms and velocity vectors in the A–B vertical cross sections.

five steady spokes at $\gamma = 1$, seven steady spokes at $\gamma = 2$ and nine spokes pattern at $\gamma = 6$ were calculated. For higher γ, higher numbers of spokes were resulted, but they became unstable and difficult to describe. When the magnetic field strength γ attains about 10, flow becomes oscillatory without any particular structures.

Fig. 14(a)–(d) show the corresponding temperature contours at various γ parameter. The isothermal contours at $R = 0.9$ are displayed in a plane vs. a circumferential angle ψ. Numbers of regular structures appear in the lower half of cylinder at $\gamma \geqslant 0$. Angular structures for $\gamma \geqslant 1$ are regular and steady with time, although not shown. At $10 > \gamma > 6$ angular structures were oscillating with time. Above $\gamma = 10$ non-structured, unsteady 3D flow was resulted.

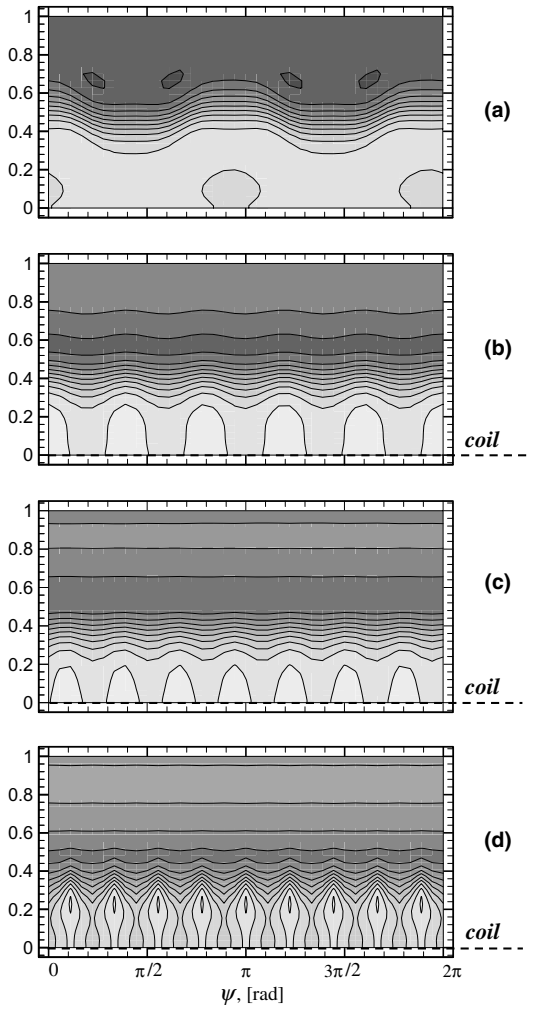

Fig. 14. Temperature contours at ($R = 0.9$) along the cylinder wall at $Z_c = 0$, $Ra = 1.52 \times 10^4$, $Pr = 0.71$ and at (a) $\gamma = 0$, (b) $\gamma = 1$, (c) $\gamma = 2$ and (d) $\gamma = 6$, respectively.

4. Conclusion

Three-dimensional numerical analysis was carried out for convection of air in a vertical cylindrical enclosure under a magnetic field. The effect of various parameters was tested such as the Rayleigh number Ra, magnetic field strength γ and coil elevation Z_c. In this configuration it is possible to control the flow mode and heat transfer rate with magnetic field. The highest Nusselt number was found at around $Z_c = 0.4$. Almost axi-symmetric stable convection or even near the conduction state was obtained for the coil near the top plate of the cylinder. On the other hand, strong and oscillatory convection was resulted with the magnetic coil located near the bottom plate of the cylinder.

References

[1] M. Faraday, On diamagnetic conditions of flame and gases, Philos. Mag. J. Sci. 31 (1847) 401–421.
[2] L. Pauling, R.E. Wood, J.H. Sturdivant, An instrument for determining the partial pressure of oxygen in a gas, J. Am. Chem. Soc. 68 (1946) 795–798.
[3] D. Braithwaite, E. Beaugnon, R. Tournier, Magnetic controlled convection in a paramagnetic fluid, Nature 354 (1991) 134–136.
[4] N.I. Wakayama, Behavior of flow under gradient magnetic fields, J. Appl. Phys. 69 (1991) 2734–2736.
[5] N.I. Wakayama, Effect of decreasing magnetic field on the flow of nitrogen gas, Chem. Phys. Lett. 185 (1991) 449–451.
[6] N.I. Wakayama, Magnetic promotion of combustion in diffusion flames, Combust. Flame 93 (1993) 207–214.
[7] N.I. Wakayama, T. Okada, J. Okano, T. Ozawa, Magnetic promotion of oxygen reduction reaction with Pt catalyst in sulfuric acid solutions, Jpn. J. Appl. Phys. 40 (2001) 269–271.
[8] M. Wakayama, N.I. Wakayama, Magnetic acceleration of inhaled and exhaled flows in breathing, Jpn. J. Appl. Phys. 39 (2001) 262–264.
[9] Y. Ikezoe, N. Hirota, J. Nakagawa, K. Kitazawa, Making water levitate, Nature 393 (1998) 749–750.
[10] Y. Ikezoe, N. Hirota, T. Sakihama, K. Mogi, H. Uetake, T. Homma, J. Nakagawa, H. Sugawara, K. Kitazawa, Acceleration effect of the rate of dissolution of oxygen in a magnetic field, J. Jpn. Inst. Appl. Magnet. 22 (1998) 821–824.
[11] S. Maki, T. Tagawa, H. Ozoe, Natural convection of air in a shallow cylinder of the aspect ratio three under a high magnetic field, Proceedings of Advances in Computational Heat Transfer, 2, 2001, pp. 851–857.
[12] T. Tagawa, H. Ozoe, K. Inoue, M. Ito, K. Sassa, S. Asai, Transient characteristics of convection and diffusion of oxygen gas in an open vertical cylinder under magnetizing and gravitational forces, Chem. Eng. Sci. 56 (2001) 4217–4223.

[13] T. Tagawa, H. Ozoe, Convective and diffusive phenomena of air in a vertical cylinder under strong magnetic field, Numer. Heat Transfer, Part B 41 (2002) 1–14.
[14] T. Tagawa, R. Shigemitsu, H. Ozoe, Magnetizing force modeled and numerically solved for natural convection of air in a cubic enclosure: effect of the direction of the magnetic field, Int. J. Heat Mass Transfer 45 (2002) 267–277.
[15] B. Bai, A. Yabe, J. Qi, N.I. Wakayama, Quantitative analysis of air convection caused by magnetic–fluid coupling, Am. Inst. Aeronaut. Astronaut. J. 37 (1999) 1538–1543.
[16] P. Filar, M. Kaneda, T. Tagawa, H. Ozoe, J.S. Szmyd, Numerical analysis of air convection in a vertical cylinder heated and cooled from a side wall under a strong magnetic field, Prog. Comput. Fluid Dynamics, in press.
[17] H. Ozoe, K. Toh, A technique to circumvent a singularity at a radial center with application for a three-dimensional cylindrical system, Numer. Heat Transfer, Part B 33 (3) (1998) 355–365.
[18] Thermophysical Properties Handbook, Yokendo Ltd., Tokyo, 2000.